Journal of Molecular Structure 1146 (2017) 814–820

Contents lists available at ScienceDirect

Journal of Molecular Structure

journal homepage: http://www.elsevier.com/locate/molstruc

An investigation of the effect of migratory type corrosion inhibitor on mechanical properties of zeolite-based novel geopolymers

Nestor Ulloa Auqui [a], Haci Baykara [a, b, *], Andres Rigail [a], Mauricio H. Cornejo [a, b], Jose Luis Villalba [a]

[a] Facultad de Ingeniería Mecánica y Ciencias de la Producción, Escuela Superior Politécnica del Litoral, ESPOL, Campus Gustavo Galindo Km 30.5 Vía Perimetral, Guayaquil, Ecuador
[b] Center of Nanotechnology Research and Development (CIDNA), Escuela Superior Politécnica del Litoral, ESPOL, Campus Gustavo Galindo Km 30.5 Vía Perimetral, Guayaquil, Ecuador

ARTICLE INFO

Article history:
Received 4 May 2017
Received in revised form
14 June 2017
Accepted 14 June 2017
Available online 17 June 2017

Keywords:
Corrosion inhibitors
Alkali activation
Natural zeolite
Geopolymer
Compressive strength

ABSTRACT

The effects of migratory type corrosion inhibitor and curing time on the thermal stability and mechanical properties of Ecuadorian natural zeolite-based geopolymers were evaluated. Geopolymer samples were prepared by alkali activation of the natural zeolite by 8 M NaOH solution and calcium hydroxide $Ca(OH)_2$ 1–3 wt%, with an activator/binder ratio of 0.6. The geopolymer samples cured for 24 h at 40 °C and then for 6 days more at room temperature showed the compressive strength values in a range of 3–5,5 MPa. Mineralogical analysis of natural zeolite obtained by XRD is as follows: Mordenite (~67%), quartz (~27%) and amorphous (~6%). SEM-EDS micrographs analysis of geopolymers revealed the presence of Na and Ca which proves the incorporation of the activators, NaOH and $Ca(OH)_2$. The compressive strength values obtained indicate that the use of alkali activation of natural zeolites is an effective method for the synthesis of geopolymers. The mechanical properties of geopolymers were slightly but not adversely affected by the addition of the migratory corrosion inhibitor, MCI-2005 NS. These results will be used in future research on geopolymer concrete with embedded reinforcing steel.

1. Introduction

Ordinary Portland cement (OPC) concrete has traditionally been used as building material worldwide, reaching an annual global cement production of 2.8 million tons, and is expected to increase to about 4 million tons per year [1,2]. Studies predict that by 2050 world demand for OPC production will sharply rise to 5.5 Gt/year [1,3]. This would imply significant large environmental impacts and massive consumption of natural resources [1,2,4].

It is calculated that ca. 0.54 tons of CO_2 per ton of clinker is released during cement production and 0.46 tons of CO_2 emitted as the result of burning combustible to supply the energy needed for this process. So it can be said that only cement production can contribute approximately 7% of human-driven global CO_2 emissions [1,4–8].

Global warming problem and greenhouse gas effect lead to numerous investigations in attempts to develop new binders without cement to reduce CO_2 emissions in the production of OPC, replacing the clinker with supplementary cementitious materials giving rise to the development of new alternative materials [8]. These new materials are called geopolymers and first developed by Joseph Davidovits in 1982 [9]. Geopolymers are tetrahedral three-dimensional inorganic aluminum silicate inorganic polymers composed of $[AlO_4]$ and $[SiO_4]$ which are mainly prepared from aluminum silicates or of industrial wastes such as fly ash [3,10–12], natural pozzolana [13,14], metakaolin [15,16] and natural zeolites [4,17–19], etc. Geopolymers are prepared by the activation of aluminum silicates mentioned by an alkali silicate solution in a highly alkaline condition [9,20,21].

Geopolymers are a class of aluminosilicate binder materials synthesized by a condensation reaction called geopolymerization of aluminosilicate minerals (such as industrial solid waste, calcinated clays, natural minerals and so on) with solutions of alkaline activator at or above room temperature [22]. They have been considered gradually to be potentially revolutionary materials in

* Corresponding author. Facultad de Ingeniería Mecánica y Ciencias de la Producción, Escuela Superior Politécnica del Litoral, ESPOL, Campus Gustavo Galindo Km 30.5 Vía Perimetral, Guayaquil, Ecuador.
E-mail address: hacibaykara@gmail.com (H. Baykara).

http://dx.doi.org/10.1016/j.molstruc.2017.06.066
0022-2860/

recent years to obtain great advantages like replacement material for OPC, in terms of its thermal, mechanical and chemical resistance properties are usually similar and even superior [15].

Various authors have studied the use of corrosion inhibitors in OPC concrete, mainly for reinforced steel corrosion embed in concrete, from coastal regions where the climate is characterized by contaminants such as chlorine ions (Cl^-) and carbon dioxide (CO_2) [23–28], this affects in the detachment an delayering of steel and as a consequence, the detriment of concrete in reinforced structures. The use of corrosion inhibitors is a method to prevent and delay the apparition of corrosion in concrete reinforced bars [29,30]. One of the possible definitions of corrosion inhibitors is given by the ISO 8044: 1989 that establishes that the material is a chemical substance that, in certain quantity, slows down the corrosion rate without a change in the concentration of any other corrosion agent [31]. Recently, the corrosion inhibitors are easy to implement for the protection of reinforced steel in concrete but, to be considered viable, these additives must not only prevent or delay the apparition of the corrosion, but also must not have any harming effect over the properties of concrete like power, curing time, workability and durability [27,32].

Over the last decades, new types of mixtures and additives have been developed in order to reduce the risk of steel corrosion in reinforced concrete. Some corrosion inhibitors can be mixed into fresh concrete, giving greater corrosion protection. Other types of corrosion inhibitors may be applied to the surface of existing concrete structures [33]. The great majority of investigations that have been mentioned above mainly focus on the study of corrosion and physical-chemical properties in reinforced concrete beams of OPC.

The effect of the addition of corrosion inhibitors on the properties of geopolymers has not been investigated yet. However, this contribution will only investigate whether the migratory type corrosion inhibitor has an effect or not in three types of geopolymer blends prepared. Therefore, the main objective of the present study is to examine the effects of addition of amine carboxylate migratory corrosion inhibitor (MCI-2005 NS) on mechanical properties of geopolymers synthesized by alkali activation of Ecuadorian natural zeolite-rich tuff with sodium hydroxide NaOH and $Ca(OH)_2$ (1–3 wt %). All the synthesized new geopolymer samples were characterized by TGA/DSC (different heating rates), XRD, SEM-EDS methods.

2. Experimental part

2.1. Materials

Ecuadorian natural zeolite-rich tuff was supplied by Zeolitas S.A. Company, which is located in the city of Guayaquil-Ecuador. Zeolite was received as small rocks, which were milled to obtain a particle size of 200 μm and dried at 60 °C for 24 h. After this process, the samples were pulverized to a particle size of <45 μm. The zeolite powder obtained was used without any further treatment.

The amine carboxylates technology based migratory type corrosion inhibitor, MCI-2005 NS was gently supplied by Cortec® Corporation. MCI-2005 NS is a liquid additive that protects reinforcing steel, carbon steel, galvanized steel and other metals embedded in concrete from corrosion induced by carbonation, chlorides and atmospheric attack. This inhibitor has the following specifications: pH: 11–12 (1% solution), non-volatile content: 25–30% and density: 9.9–10 lb/gal.

Alkaline activators were selected according to the literature in which they mention high compressive strength [34–38], the use of NaOH and $Ca(OH)_2$ as moisturizing at different percentages. NaOH was used as pallets with a purity of 99.0% supplied by Merck Millipore and $Ca(OH)_2$ powder with a purity grade of 97.2% supplied by J.T. Baker origin.

2.2. Synthesis, testing and characterization

The natural zeolite was activated with an 8 M NaOH solution with different percentages of $Ca(OH)_2$, (1–3 wt% of the mass of zeolite) to prepare each geopolymer sample (ZG). The reactive and zeolite were mixed by adding the MCI-2005 NS corrosion inhibitor in the amount of 1 l/m^3, according to product specifications. Samples were prepared at the constant activator/binding ratio of 0.6. A HOBART model N-50 mechanical mixer with mixing speeds and agitator type according to the standard ASTM C305 [39], was used to mix the components and prepare the geopolymer samples. The geopolymer obtained paste was poured into $50 \times 50 \times 50$ mm cubic molds according to standard ASTM C109/C109 M-05 [40,41] and covered with a plastic packing to prevent dehydration, excessive moisture loss and thermal stress in the geopolymer structure [42], cured for 24 h at 40 °C, and then further demolded and cured at room temperature for 6 days more.

To determine the particle size reliability, a random sample of zeolite powder was analyzed on the Mastersizer 2000, Hydro SM equipment. The distribution of the natural zeolite particle size is presented in Fig. 1. According to this figure, the natural zeolite studied has particles in the range of $1-45$ μm. Most of these particles are in the range of 10 *to* 20 μm and approximately 90% of the particles have a size of >12 μm.

Compressive strength tests were performed using a SHIMADZU Universal Testing Machine model UTM-600KN to the cubes for the aforementioned curing times in order to evaluate the compressive force according to ASTM C109/C109 M-05 [40].

The microstructure, elemental analysis and mineral content of the zeolite as well as the activated materials was carried out by scanning electron microscopy (SEM) equipped by energy dispersive spectrometer (EDS), and X-ray diffractometry methods, respectively. SEM-EDS micrographs were obtained using a Scanning Electron Microscope equipped with a FEI brand Dispersive Energy Spectrometer model Inspect S. For the SEM-EDS analysis, an aluminum sample holder was used on an adhesive carbon disk to improve the electron transfer. No metal coating was used on the sample for analysis, an acceleration voltage of 12.5 KV and an atmosphere of 80 Pa of water vapor was used, with two spot sizes for the images and a spot size of 4 for The EDS analysis.

A PANalytical® X'Pert PRO X-ray diffractometer (XRD) was used in conjunction with X'Pert High Score Plus® software to quantify the mineral and amorphous contents of both zeolite and geopolymers. The operating conditions were 40 mA and 45 KV, with step size of 0.02°, a conventional X-ray tube (Cu_Kα radiation) and a multi-channel X'Celerator detector with anti-dispersion protection. In addition, the Rietveld method was used to quantify the mineralogical and amorphous content according to experimental

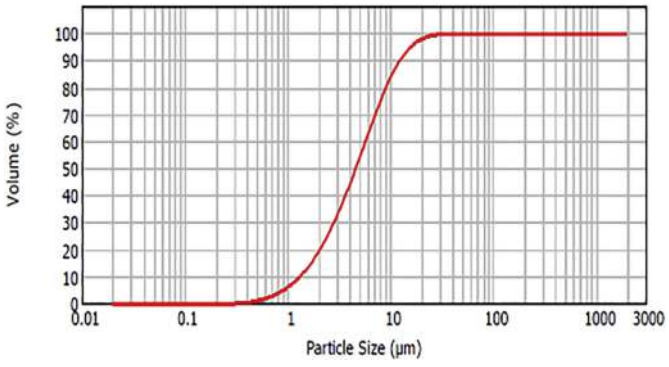

Fig. 1. Particle size distribution of natural zeolite powder prepared.

techniques found elsewhere [43–46]. Samples with a particle size lower than 45 μm was used for XRD analysis. The refinement cycle consisted of global parameters like overall zero shit, specimen displacement, background, and scale factors at the beginning, and then cell parameters. Finally, profile parameters were refined. After several refinement cycles, if the agreement indices like weighted-R percent (Rwp) and goodness of fit (GOF) are less than 12 and 5, respectively, then results are accepted. The agreement indices Rwp and GOF obtained for refinement are in the acceptable range with the values of 11,66 and 1,198, respectively.

The starting structure models were obtained from Inorganic Crystal Structure Database (ICSD), Mordenite, 98841; quartz, 18172; calcite, 16710, and ZnO which NIST code is 674b was used as internal standard. 10 wt% ZnO of each sample was used as internal standard for the quantitative analysis of zeolite and its corresponding geopolymers [45].

A TA Instruments STD Q-600 brand simultaneous thermogravimetric analysis and differential scanning calorimetry (TGA-DSC) system was used for the thermal stability analyses. Alumina crucibles were used for both reference and samples. The sample was taken in powder and for each analysis the quantity of about 8–10 mg was used. The test was performed with a temperature range from ambient to 1000 °C, at different heating rates of 5, 7.5, 10, 15 and 20 °C/min, with a nitrogen flow rate of 100 mL/min [47]. Advantage TA Universal Analysis 4.5A software was used to analyze the data obtained.

3. Results and discussions

3.1. XRD analysis of zeolite and its corresponding geopolymer

The diffractogram (see Fig. 2) of the natural zeolite shows the presence of the crystalline phases in a greater quantity of mordenite (~67%) and a smaller quantity of quartz (~27%). The halo that occurs between 20° and 30° (2θ) indicates the presence of the fraction of amorphous content (~6%) [34]. In Fig. 2, it is observed that mordenite is the most abundant phase in the as-received sample presenting several peaks, although quartz shows the highest peak. Fig. 3 shows XRD analysis of ZG3 (with inhibitor) coded geopolymer, which showed the highest compressive strength. XRD analysis of the sample was carried two months later after compressive strength test was done. As seen, alkali activation had gone successfully and all the mordenite (MOR) and a great

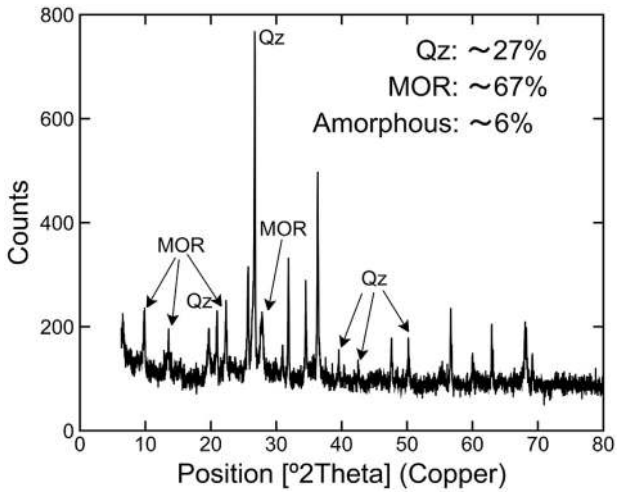

Fig. 2. XRD analysis of the raw material, Ecuadorian natural zeolite (**MOR**: Mordenite, **Qz**: Quartz, non-assigned peaks are belong to the internal standard, ZnO).

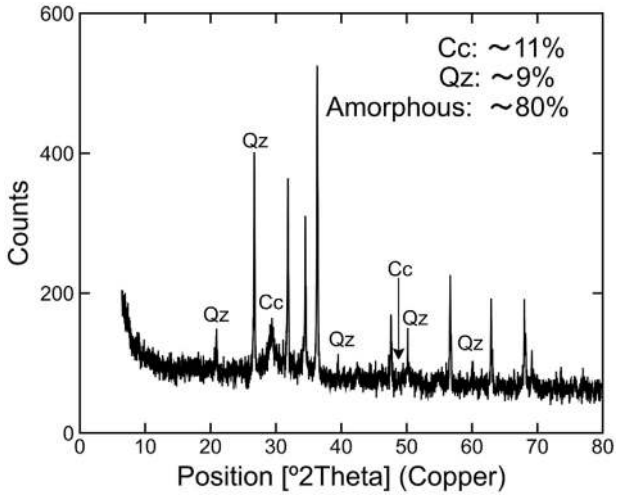

Fig. 3. XRD analysis of ZG3-with inhibitor (**Qz**: Quartz, **Cc**: Calcium carbonate, non-assigned peaks are belong to the internal standard, ZnO).

percentage of quartz (Qz) were disappeared. So amorphous content has increased to the value of ~80%, but a new crystalline phase, calcium carbonate (Cc) was formed with a decrease of the content of SiO_2 (see Fig. 3). The amorphization is attributed to the formation of geopolymer [9,12,16,34]. Calcium carbonate can be formed by the reaction between the excess of $Ca(OH)_2$ and CO_2 [1,12,20,48]. It is worth to note that the highest peak belongs to the internal standard, ZnO (In Figs. 2 and 3, non-assigned/labeled peaks). These suggest that almost all amount of mordenite reacted with alkali solution transforming into amorphous aluminosilicate, which was the most abundant compound after reaction times.

3.2. Mechanical properties

Compressive strength (see Table 1) of ZG (each sample were triplicated) samples with and without corrosion inhibitor by presence of 1,2 and 3 wt% of $Ca(OH)_2$ was measured after a curing time of 24 h and aging for 6 days. Geopolymer samples were coded as ZG1, ZG1 and ZG3 with respect to the $Ca(OH)_2$ content, respectively. The quantity of corrosion inhibitor, MCI-2005 NS was kept constant as 125 μL for the preparation each geopolymer cube with the volume of 125 cm^3 according to the specifications of the inhibitor.

Table 1 shows the results of the average compressive strength of the analyzed samples of synthesized geopolymers. In general, it can be observed that the synthesized geopolymers show an increase in the compressive strength when there is an increase in the percentage of $Ca(OH)_2$ and curing time. During the first 24 h, it was cured at 40 °C, and then cured at room temperature for 6 days to avoid dehydration, excessive moisture loss, and thermal stress in the geopolymer structure (see Fig. 4), which causes lower

Table 1
Results of the compressive strength.

Sample	$Ca(OH)_2$ (wt%)	Activator/binder ratio	Compressive strength (MPa)			
			No Inhibitor		Inhibitor	
			1 day	7 day	1 day	7 day
ZG1	1	0.6	3.20	4.35	3.32	4.33
ZG2	2	0.6	3.60	4.83	3.62	4.90
ZG3	3	0.6	3.87	5.24	3.85	5.30

ZG: Zeolite Geopolymer.

Fig. 4. Synthesized geopolymers (5 × 5 × 5 cm^3 cubes).

compressive strength and cracks in the structure of geopolymer samples. It can be deduced that the addition of the corrosion inhibitor in the blends to synthesize the geopolymers does not cause any effect or reduction in the main objective compressive strength of the present investigation. The maximum compressive strength was recorded in samples ZG3, reaching 5.30, and 5.24 MPa on average, with and without corrosion inhibitor respectively, for 7 days of curing time at room temperature.

3.3. Characterization by scanning electron microscopy and dispersive energy spectroscopy (SEM-EDS)

The following figures show the micrographs obtained of the zeolite without activation by means of SEM (see Fig. 5), the geopolymer (ZG3-with inhibitor) that registered higher compressive strength (see Fig. 6) and a sample of the geopolymer, residue of the calcined TGA analysis at a temperature ramp of 20 °C/min (see Fig. 7). These micrographs were taken with the objective of analyzing the chemical composition and microstructural evolution of the geopolymer. Small pieces of untreated and calcined geopolymer samples (after the TGA analysis) were taken for the SEM-EDS analysis.

Fig. 6 shows the SEM micrograph and the EDS of the geopolymer sample coded as ZG3. As seen, the incorporation of Na, Ca which come from the activators, and the percentages of the other elements have been detected. Furthermore, a matrix of very dense products and very little porosity can be observed. Some crystalline phases can also be observed which can be attributed to SiO_2 and nonreacted/nonactivated mordenite (early age geopolymer).

3.4. Thermogravimetric analysis and differential scanning calorimetry (TGA/DSC)

TGA/DSC analyzes were performed at different heating rates, to one of the resulting powdered geopolymer samples after the compressive strength test. The results of thermogravimetry (TG) are presented in Fig. 8. It can be seen that all analyzes showed similar characteristic trends up to 1000 °C. A significant mas loss was observed between room temperature and 300 °C in each analysis, which is because of the evaporation of the absorbed water, and the water within the pores of geopolymers [49,50]. The additional mass loss was observed between 300 – 600 °C, the is attributed to the dehydroxylation of the Si-OH and Al-OH groups in geopolymeric structure [47,49–52]. The 3% mass loss between 600 °C and 850 °C can be attributed to decarbonation of potential byproducts like $CaCO_3$ and Na_2CO_3. Since the excess of the activator is used to prepare geopolymer samples the carbonates mentioned above can be formed by the reaction of alkali activators and CO_2 [12,31,49,50,53]. So the main mass loss is because of existence of water due to the short term curing conditions (24 h and 7 days), and it can be reduced by long-term curing conditions.

All analyzes exhibited similar DSC thermograms, however, as the heating rate increases, the endothermic peak increases considerably and vice versa for the exothermic peak (decreases), as can be seen in Fig. 9. Two traces were observed characteristic in all thermograms; a large endothermic peak in the region of low temperature and a small exothermic peak in the region of high temperature.

The large endothermic peaks in the DSC curves ranged from

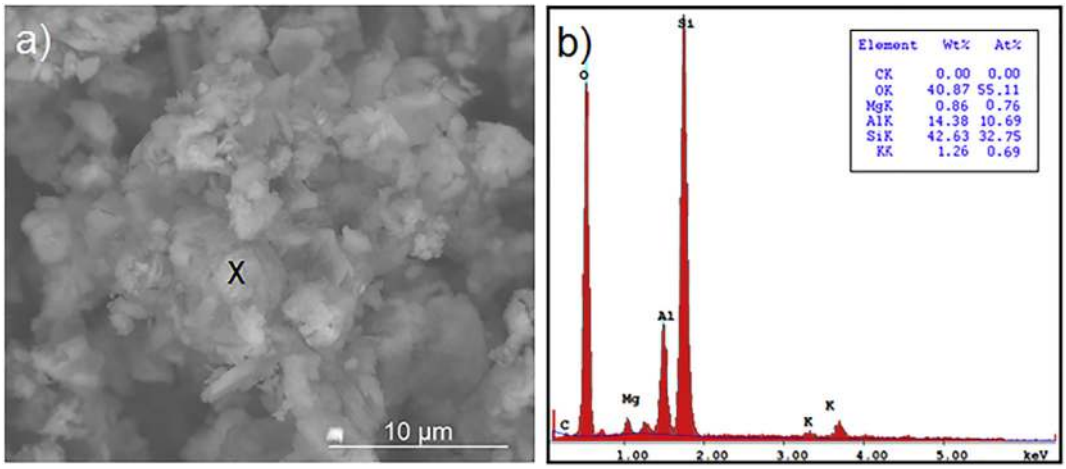

Fig. 5. SEM-EDS analysis of Ecuadorian natural zeolite. a) SEM micrograph of natural zeolite; b) Single-point elemental analysis of natural zeolite by EDS.

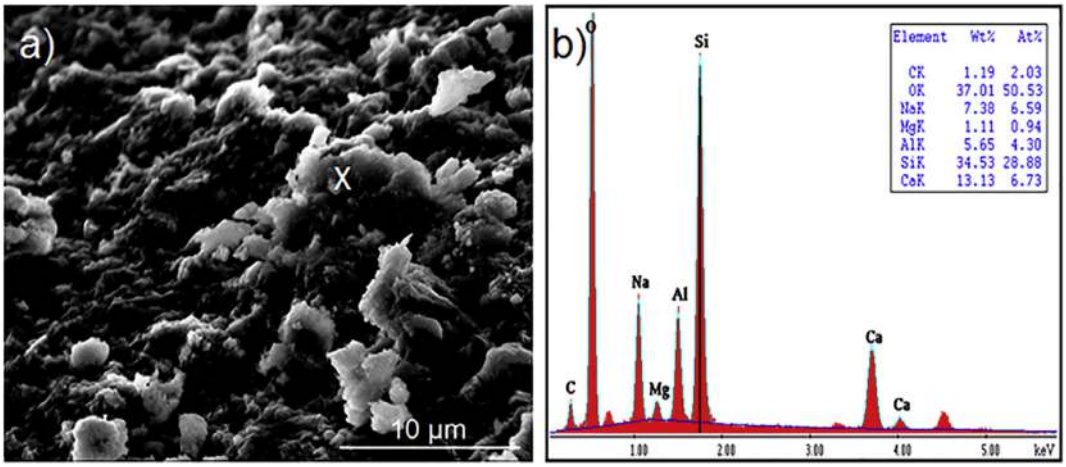

Fig. 6. SEM-EDS analysis of ZG3. a) Microphotograph of the geopolymer, ZG3, b) Single-point elemental analysis of ZG3 by EDS.

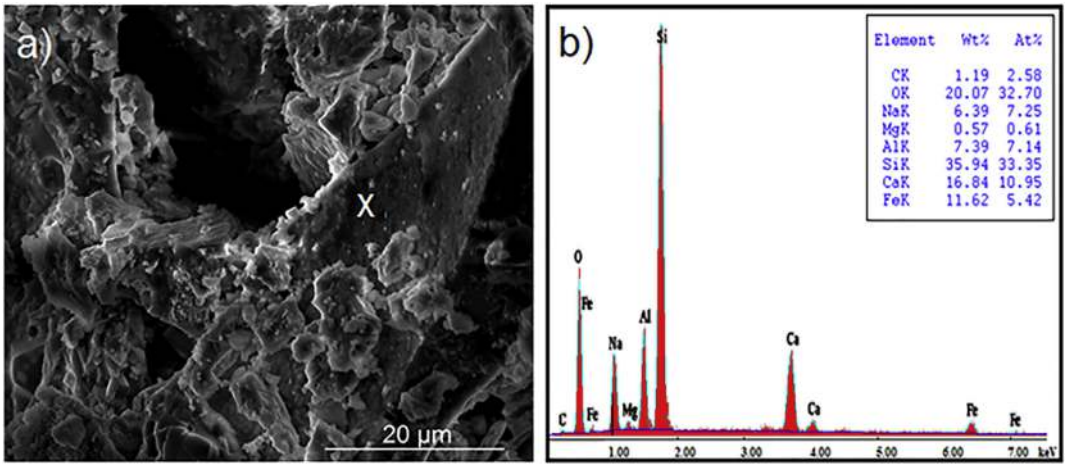

Fig. 7. a) SEM-EDS analysis of thermally analyzed (20 °C/min) ZG3 sample. b) Single-point elemental analysis of thermally analyzed ZG3 sample by EDS.

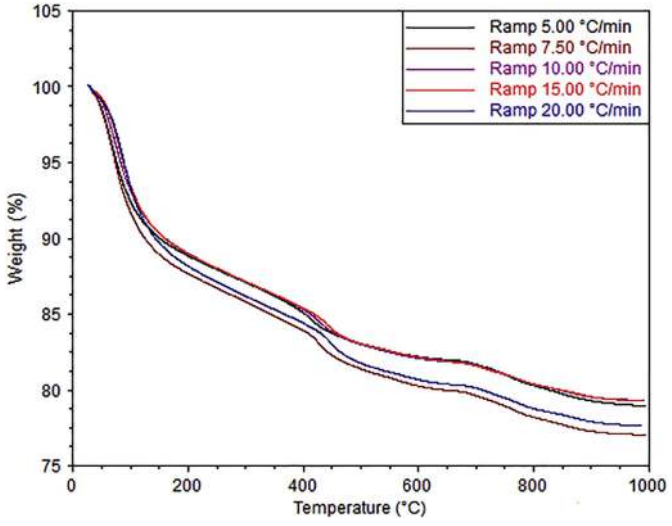

Fig. 8. Thermograms for ZG3-with inhibitor, (at various heating rates) from room temperature up to 1000 °C.

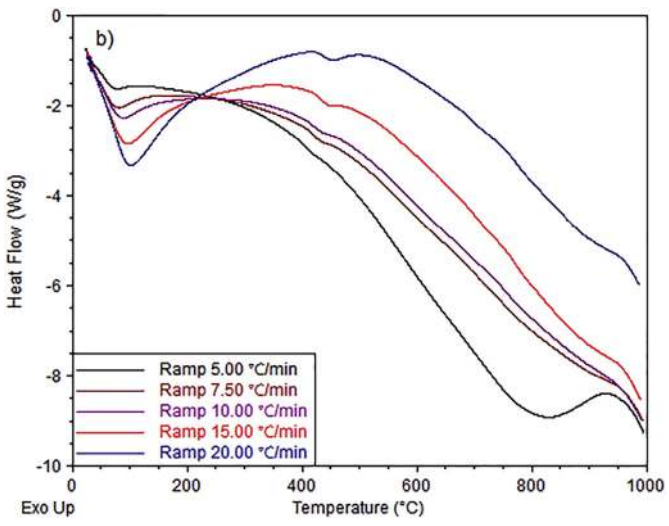

Fig. 9. DSC thermograms for ZG3-with inhibitor, (at various heating rates) from room temperature up to 1000 °C.

40 °C to 300 °C and were attributed to the evaporation of free water in the geopolymer, as indicated by thermogravimetric analysis. In the high temperature region of the exothermic peak (around 950 °C), this may be caused by the crystallization or re-arrangement of the mineral phases found in the sample, as indicated in the literature [47,54], or it may also be the formation of new phases [55]. As seen in Fig. 9, all the heat flows show a similar tendency corresponding of each thermal event, but the lower heating rates especially 5 °C shows a very good resolution with a very good sensitivity. For example the exothermic peak between 850 and 1000 °C can be clearly seen at 5 °C of heating rate, but not at the other heating rates. So the lower heating rates applied, the more precise in thermal events obtained [56,57].

4. Conclusions

A curing time outlasting 24 h can provoke structural defects of the geopolymer by forming cracks due to excessive and rapid dehydration. So, a curing time up to 24 h, and a curing temperature of 40 °C or room temperature can be applied to the geopolymer samples prepared by alkali activation of Ecuadorian natural zeolite.

The addition of MCI-2005 NS corrosion inhibitor in geopolymer structure doesn't affect adversely the mechanical properties of geopolymer samples.

The excessive use of one the activators, $Ca(OH)_2$ as powder causes the inevitable result, carbonation, both in the short and long terms.

The lower heating rates in TGA/DSC analysis especially 5 °C/min increased the precise of thermal characterization of the samples.

The presence of Na, Ca detected in SEM-EDS analysis proves the incorporation of the activators, NaOH and $Ca(OH)_2$ in geopolymer synthesis with and without corrosion inhibitor.

Acknowledgments

The authors thank the Laboratorio de Ensayos de Materiales (LEMAT) of the Escuela Superior Politécnica de Litoral (Ecuador), especially Dr. Martín Mendoza, Ing. Julio Cáceres and Ing. José Pilataxi, for their help in XRD, TGA-DSC, SEM/EDS analyses.

Appendix A. Supplementary data

Supplementary data related to this article can be found at http://dx.doi.org/10.1016/j.molstruc.2017.06.066.

References

[1] M. Schneider, M. Romer, M. Tschudin, H. Bolio, Sustainable cement production-present and future, Cem. Concr. Res. 41 (2011) 642–650, http://dx.doi.org/10.1016/j.cemconres.2011.03.019.
[2] D.A. Salas, A.D. Ramirez, C.R. Rodríguez, D.M. Petroche, A.J. Boero, J. Duque-Rivera, Environmental impacts, life cycle assessment and potential improvement measures for cement production: a literature review, J. Clean. Prod. 113 (2016) 114–122, http://dx.doi.org/10.1016/j.jclepro.2015.11.078.
[3] M. Babaee, A. Castel, Chloride-induced corrosion of reinforcement in low-calcium fly ash-based geopolymer concrete, Cem. Concr. Res. 88 (2016) 96–107, http://dx.doi.org/10.1016/j.cemconres.2016.05.012.
[4] B.W. Jo, J.S. Choi, K.W. Yoon, J.H. Park, Material characteristics of zeolite cement mortar, Constr. Build. Mater. 36 (2012) 1059–1065, http://dx.doi.org/10.1016/j.conbuildmat.2012.06.061.
[5] C. Gunasekara, D.W. Law, S. Setunge, J.G. Sanjayan, Zeta potential, gel formation and compressive strength of low calcium fly ash geopolymers, Constr. Build. Mater. 95 (2015) 592–599, http://dx.doi.org/10.1016/j.conbuildmat.2015.07.175.
[6] P. Duan, C. Yan, W. Zhou, W. Luo, Fresh properties, mechanical strength and microstructure of fly ash geopolymer paste reinforced with sawdust, Constr. Build. Mater. 111 (2016) 600–610, http://dx.doi.org/10.1016/j.conbuildmat.2016.02.091.
[7] A. Petrillo, R. Cioffi, C. Ferone, F. Colangelo, C. Borrelli, Eco-sustainable geopolymer concrete blocks production process, Agric. Agric. Sci. Procedia 8 (2016) 408–418, http://dx.doi.org/10.1016/j.aaspro.2016.02.037.
[8] K.H. Yang, J.K. Song, K. Il Song, Assessment of CO2 reduction of alkali-activated concrete, J. Clean. Prod. 39 (2013) 265–272, http://dx.doi.org/10.1016/j.jclepro.2012.08.001.
[9] J. Davidovits, Geopolymers, J. Therm. Anal. 37 (1991) 1633–1656, http://dx.doi.org/10.1007/BF01912193.
[10] C. Monticelli, M.E. Natali, A. Balbo, C. Chiavari, F. Zanotto, S. Manzi, M.C. Bignozzi, A study on the corrosion of reinforcing bars in alkali-activated fly ash mortars under wet and dry exposures to chloride solutions, Cem. Concr. Res. 87 (2016) 53–63, http://dx.doi.org/10.1016/j.cemconres.2016.05.010.
[11] P. Sukmak, S. Horpibulsuk, S.L. Shen, P. Chindaprasirt, C. Suksiripattanapong, Factors influencing strength development in clay-fly ash geopolymer, Constr. Build. Mater. 47 (2013) 1125–1136, http://dx.doi.org/10.1016/j.conbuildmat.2013.05.104.
[12] W. Mozgawa, J. Deja, Spectroscopic studies of alkaline activated slag geopolymers, J. Mol. Struct. 924–926 (2009) 434–441, http://dx.doi.org/10.1016/j.molstruc.2008.12.026.
[13] R.H. Haddad, O. Alshbuol, Production of geopolymer concrete using natural pozzolan: a parametric study, Constr. Build. Mater. 114 (2016) 699–707, http://dx.doi.org/10.1016/j.conbuildmat.2016.04.011.
[14] M. Najimi, J. Sobhani, B. Ahmadi, M. Shekarchi, An experimental study on durability properties of concrete containing zeolite as a highly reactive natural pozzolan, Constr. Build. Mater. 35 (2012) 1023–1033, http://dx.doi.org/10.1016/j.conbuildmat.2012.04.038.
[15] B.H. Mo, H. Zhu, X.M. Cui, Y. He, S.Y. Gong, Effect of curing temperature on geopolymerization of metakaolin-based geopolymers, Appl. Clay Sci. 99 (2014) 144–148, http://dx.doi.org/10.1016/j.clay.2014.06.024.
[16] M. Sarkar, K. Dana, S. Das, Microstructural and phase evolution in metakaolin geopolymers with different activators and added aluminosilicate fillers, J. Mol. Struct. 1098 (2015) 110–118, http://dx.doi.org/10.1016/j.molstruc.2015.05.046.
[17] M.H. Cornejo, J. Elsen, C. Paredes, H. Baykara, Hydration and strength evolution of air-cured zeolite-rich tuffs and siltstone blended cement pastes at low water-to-binder ratio, Clay Miner. 50 (2015) 133–152, http://dx.doi.org/10.1180/claymin.2015.050.1.12.
[18] M. Król, J. Minkiewicz, W. Mozgawa, M. Krol, J. Minkiewicz, W. Mozgawa, IR spectroscopy studies of zeolites in geopolymeric materials derived from kaolinite, J. Mol. Struct. 1126 (2016) 200–206, http://dx.doi.org/10.1016/j.molstruc.2016.02.027.
[19] H. Baykara, M.H. Cornejo, R. Murillo, A. Gavilanes, C. Paredes, J. Elsen, Preparation, characterization and reaction kinetics of green cement: Ecuadorian natural mordenite-based geopolymers, Mater. Struct. 50 (2017), http://dx.doi.org/10.1617/s11527-017-1057-z.
[20] J. Davidovits, Environmentally driven geopolymer cement applications, in: Geopolymer 2002 Conf. (2002) 1–9.
[21] J. Davidovits, Mineral polymers and methods of making them, US4349386 A, 1982. https://www.google.com/patents/US4349386 (Accessed 12 February 2017).
[22] P. Duxson, A. Fernández-Jiménez, J.L. Provis, G.C. Lukey, A. Palomo, J.S.J. Van Deventer, Geopolymer technology: the current state of the art, J. Mater. Sci. 42 (2007) 2917–2933, http://dx.doi.org/10.1007/s10853-006-0637-z.
[23] E. Rakanta, T. Zafeiropoulou, G. Batis, Corrosion protection of steel with DMEA-based organic inhibitor, Constr. Build. Mater. 44 (2013) 507–513, http://dx.doi.org/10.1016/j.conbuildmat.2013.03.030.
[24] P. Faustino, A. Brás, T. Ripper, Corrosion inhibitors' effect on design service life of RC structures, Constr. Build. Mater. 53 (2014) 360–369, http://dx.doi.org/10.1016/j.conbuildmat.2013.11.098.
[25] A.A. Sagüés, Galvanized steel reinforcement in concrete, in: Galvaniz. Steel Reinf. Concr. (2004) 71–86. http://dx.doi.org/10.1016/B978-008044511-3/50018-9.
[26] Z. Ahmad, 12 concrete corrosion, Princ. Corros. Eng. Corros. Control (2006) 609–646, http://dx.doi.org/10.1016/B978-075065924-6/50013-1.
[27] M. Büchler, Corrosion Inhibitors for Reinforced Concrete, Elsevier Ltd, 2005, http://dx.doi.org/10.1533/9781845690434.190.
[28] J.M. Gaidis, Chemistry of corrosion inhibitors, Cem. Concr. Compos. 26 (2004) 181–189, http://dx.doi.org/10.1016/S0958-9465(03)00037-4.
[29] M. Forsyth, M.Z. Lourenco, Corrosion and protection of steel in concrete, Corros. Mater. 22 (1997) 13–16, http://dx.doi.org/10.1533/9781845693398.136.
[30] M. Ormellese, M. Berra, F. Bolzoni, T. Pastore, Corrosion inhibitors for chlorides induced corrosion in reinforced concrete structures, Cem. Concr. Res. 36 (2006) 536–547, http://dx.doi.org/10.1016/j.cemconres.2005.11.007.
[31] T.A. Söylev, M.G. Richardson, Corrosion inhibitors for steel in concrete: state-of-the-art report, Constr. Build. Mater. 22 (2008) 609–622, http://dx.doi.org/10.1016/j.conbuildmat.2006.10.013.
[32] V. Saraswathy, H.W. Song, Improving the durability of concrete by using inhibitors, Build. Environ. 42 (2007) 464–472, http://dx.doi.org/10.1016/j.buildenv.2005.08.003.
[33] G. De Schutter, L. Luo, Effect of corrosion inhibiting admixtures on concrete properties, Constr. Build. Mater. 18 (2004) 483–489, http://dx.doi.org/10.1016/j.conbuildmat.2004.04.001.
[34] C. Villa, E.T. Pecina, R. Torres, L. Gómez, Geopolymer synthesis using alkaline activation of natural zeolite, Constr. Build. Mater. 24 (2010) 2084–2090, http://dx.doi.org/10.1016/j.conbuildmat.2010.04.052.

[35] C. Karakurt, L.B. Topu, Effect of blended cements with natural zeolite and industrial by-products on rebar corrosion and high temperature resistance of concrete, Constr. Build. Mater. 35 (2012) 906–911, http://dx.doi.org/10.1016/j.conbuildmat.2012.04.045.
[36] E.A. Ortega, C. Cheeseman, J. Knight, M. Loizidou, Properties of alkali-activated clinoptilolite, Cem. Concr. Res. 30 (2000) 1641–1646, http://dx.doi.org/10.1016/S0008-8846(00)00331-8.
[37] T. Suwan, M. Fan, N. Braimah, Micro-mechanisms and compressive strength of Geopolymer-Portland cementitious system under various curing temperatures, Mater. Chem. Phys. 180 (2016) 219–225, http://dx.doi.org/10.1016/j.matchemphys.2016.05.069.
[38] G.S. Ryu, Y.B. Lee, K.T. Koh, Y.S. Chung, The mechanical properties of fly ash-based geopolymer concrete with alkaline activators, Constr. Build. Mater. 47 (2013) 409–418, http://dx.doi.org/10.1016/j.conbuildmat.2013.05.069.
[39] ASTM C305-11, Standard Practice for Mechanical Mixing of Hydraulic Cement Pastes and Mortars of Plastic Consistency, ASTM International, 2011, pp. 1–3, http://dx.doi.org/10.1520/C0305-13.2.
[40] ASTM C109/C109M-05, Standard Test Method for Compressive Strength of Hydraulic Cement Mortars, 2005, http://dx.doi.org/10.1520/C0109_C0109M-05.
[41] M. Cabinets, M. Rooms, B. Statements, D. Mass, Standard test method for compressive strength of hydraulic cement mortars (using 2-in. or [50-mm] cube specimens) 1, Chem. Anal. (2010) 1–9, http://dx.doi.org/10.1520/C0109.
[42] M.F. Nuruddin, S.A. Qazi, A. Kusbiantoro, N. Shafiq, Utilisation of waste material in geopolymeric concrete, Proc. Inst. Civ. Eng. Constr. Mater. 164 (2011) 315–327, http://dx.doi.org/10.1680/coma.2011.164.6.315.
[43] R. Snellings, G. Mertens, Ö. Cizer, J. Elsen, Early age hydration and pozzolanic reaction in natural zeolite blended cements: reaction kinetics and products by in situ synchrotron X-ray powder, Cem. Concr. Res. 40 (2010) 1704–1713, http://dx.doi.org/10.1016/j.cemconres.2010.08.012.
[44] L. Machiels, F. Morante, R. Snellings, B. Calvo, L. Canoira, C. Paredes, J. Elsen, Zeolite mineralogy of the cayo formation in Guayaquil, Ecuador, Appl. Clay Sci. 42 (2008) 180–188, http://dx.doi.org/10.1016/j.clay.2008.01.012.
[45] R. Snellings, L. Machiels, G. Mertens, J. Elsen, Rietveld refinement strategy for quantitative phase analysis of partially amorphous zeolitized tuffaceous rocks, Geol. Belg. 13 (2010) 183–196.
[46] L. Machiels, D. Garcés, R. Snellings, W. Vilema, F. Morante, C. Paredes, J. Elsen, Zeolite occurrence and genesis in the Late-Cretaceous Cayo arc of Coastal Ecuador: evidence for zeolite formation in cooling marine pyroclastic flow deposits, Appl. Clay Sci. 87 (2014) 108–119, http://dx.doi.org/10.1016/j.clay.2013.10.018.
[47] M.A. Villaquirán-Caicedo, R.M. de Gutiérrez, S. Sulekar, C. Davis, J.C. Nino, Thermal properties of novel binary geopolymers based on metakaolin and alternative silica sources, Appl. Clay Sci. 118 (2015) 276–282, http://dx.doi.org/10.1016/j.clay.2015.10.005.
[48] X.Y. Zhuang, L. Chen, S. Komarneni, C.H. Zhou, D.S. Tong, H.M. Yang, W.H. Yu, H. Wang, Fly ash-based geopolymer: clean production, properties and applications, J. Clean. Prod. (n.d.) http://dx.doi.org/10.1016/j.jclepro.2016.03.019.
[49] M. Alshaaer, B. El-Eswed, R.I. Yousef, F. Khalili, H. Rahier, Development of functional geopolymers for water purification, and construction purposes, J. Saudi Chem. Soc. 20 (2016) S85–S92, http://dx.doi.org/10.1016/j.jscs.2012.09.012.
[50] R.L. Frost, M.C. Hales, W.N. Martens, Thermogravimetric analysis of selected group (II) carbonate minerals - implication for the geosequestration of greenhouse gases, J. Therm. Anal. Calorim. 95 (2009) 999–1005, http://dx.doi.org/10.1007/s10973-008-9196-7.
[51] P. He, D. Jia, M. Wang, Y. Zhou, Effect of cesium substitution on the thermal evolution and ceramics formation of potassium-based geopolymer, Ceram. Int. 36 (2010) 2395–2400, http://dx.doi.org/10.1016/j.ceramint.2010.07.015.
[52] P. Duxson, S.W. Mallicoat, G.C. Lukey, W.M. Kriven, J.S.J. van Deventer, The effect of alkali and Si/Al ratio on the development of mechanical properties of metakaolin-based geopolymers, Colloids Surfaces A Physicochem. Eng. Asp. 292 (2007) 8–20, http://dx.doi.org/10.1016/j.colsurfa.2006.05.044.
[53] M. Zhang, M. Zhao, G. Zhang, T. El-Korchi, M. Tao, A multiscale investigation of reaction kinetics, phase formation, and mechanical properties of metakaolin geopolymers, Cem. Concr. Compos. 78 (2017) 21–32, http://dx.doi.org/10.1016/j.cemconcomp.2016.12.010.
[54] H.Y. Zhang, V. Kodur, B. Wu, L. Cao, F. Wang, Thermal behavior and mechanical properties of geopolymer mortar after exposure to elevated temperatures, Constr. Build. Mater. 109 (2016) 17–24, http://dx.doi.org/10.1016/j.conbuildmat.2016.01.043.
[55] M.H. Cornejo, J. Elsen, C. Paredes, H. Baykara, Thermomechanical treatment of two Ecuadorian zeolite-rich tuffs and their potential usage as supplementary cementitious materials, J. Therm. Anal. Calorim. 115 (2014) 309–321, http://dx.doi.org/10.1007/s10973-013-3345-3.
[56] S. Maiti, S. Purakayastha, B. Ghosh, Thermal characterization of mustard straw and stalk in nitrogen at different heating rates, Fuel 86 (2007) 1513–1518, http://dx.doi.org/10.1016/j.fuel.2006.11.016.
[57] R.M. Saeed, J.P. Schlegel, C. Castano, R. Sawafta, Uncertainty of thermal characterization of phase change material by differential scanning calorimetry analysis, Int. J. Eng. Res. Technol. 5 (2016) 405–412.